Heat Treatment Effects on Microstructure, Hardness & Corrosion of Al-12Si-Cu Alloy

Asaad K. EQAL [1]*, Haidar A. HUSSEIN [2]

[1]Department of Mechanical Techniques, Amarah Technical Institute, Southern Technical University, Basrsh 62001, Iraq

[2] Department of Applied Mechanics, Engineering Technical College - Baghdad, Middle Technical University, Baghdad 10074, Iraq

*** Corresponding author E-mail: asaad.kadhim@stu.edu.iq**

Abstract

The influence of different heat treatment parameters, namely solutionizing and artificial aging conditions, on the microstructure, mechanical hardness, and corrosion resistance of Al-12Si-Cu alloy are systematically explored in this work. Solution treatment was performed at two temperatures (500°C and 530°C) and two durations (0.5 and 3 hours), and artificial aging was made at two temperatures (180°C and 310°C) over two durations (2 and 5 hours). Optical microscopy also showed interesting microstructural changes with fine grain refinement and enhanced spheroidization of the coarse eutectic Si phase and a more uniform distribution of primary intermetallic grains. These structural adjustments were identified as direct determinants of properties of the material. Maximum microhardness (155 HV) was achieved at the temperatures of 500°C/3 h solutionizing and 180°C for 5 h aging (S3), which was ascribed to successful solid solution strengthening and fine precipitation hardening. In contrast, the lowest hardness (54 HV) was obtained at the values 530°C/3 h + 310°C/5 h (S8), showing the harmful impact of over-aging at higher temperatures. Analysis of electrochemical corrosion detected a significant correlation between the corrosion resistance and treated microstructure, where conditions favoring microstructural refinement resulted in a decrease in corrosion current density. A Design of Experiments (DOE) method by way of the Taguchi L8 orthogonal array was used to find out how each parameter contributed relative to

[DOI: 10.22068/ijmse.4421]

the other variable. The analysis revealed that, whilst the aging temperature was the most influential factor to the microhardness, the solution time was the controlling factor on the surface roughness. The results demonstrate a robust determination of the main processing windows which are known to be crucial to enhance particular properties and verify the tremendous feasibility of temperature control in heat treatment process optimization in engineering the necessary trade-off between mechanical strength and corrosion performance in Al-12Si-Cu alloys.

Keywords: Al-Si-Cu alloy, heat treatment, aging, corrosion, optimization.

1. Introduction

Aluminum–silicon-based alloy systems, specially the Al-12Si aluminum alloy system, are utilized to play vital roles in the automobile, aerospace and offshore industries. They are increasingly being utilized as a result of their good castability, low density, strong specific strength and inherent corrosion performance [1–3]. The important enhancement of mechanical and thermal performance of the alloy by supplementary alloying elements like copper Cu and magnesium Mg can be achieved efficiently. More precisely, this is facilitated by efficient precipitation hardening and considerable microstructure improvement [4, 5]. In all Al-Si systems, the Al-12Si-Cu system has drawn growing criticism from practitioners for its higher strength to weight ratio, cheap fabrication cost and good preparation of complex casting geometry [6]. At least at this stage, copper can readily be introduced by direct application, and is responsible for forming the intermetallic phases Al2Cu. This is important for the process of process to strengthen the alloy by fine-tuning the solution or aging treatments [7, 8]. The resultant microstructure, particularly the shapes, sizes, and spatial areas of silicon particles, eutectic phases and strengthening precipitates, play an essential role in determining the final mechanical performance of Al-Si-Cu alloys [9, 10]. Solution treatment, typically carried out at high temperature, allows all secondary phases to completely dissolve. Automated aging subsequently causes the gradual precipitation of strengthening phases (e.g., metastable θ′ (Al_2Cu)) that are required for a significant hardness and yield strength [11]. In recent years, scientists have leaned heavily on statistical design tools (e.g., the RSM and Taguchi method) to systematically optimize complex heat treatment parameters (solution temperature, aging temperature, and time holding). For instance, Pezda et al. [12] investigated the impact of T6 heat treatment parameters on the EN AC-AlSi12CuNiMg aluminum alloy modified with strontium and cast into metal molds. The optimal solutioning was achieved at a temperature of 535 °C for a duration of 3 hours, followed by immediate quenching in water at 20 °C. This stage ensured the maximum dissolution of copper-rich and magnesium-rich phases into the aluminum matrix.. Similarly, Raju, K., et al.. [13] highlighted the heat treatment (solutionizing at 510 °C, ageing at 220 °C) of Al-15Si-6Ni-2Cu alloy induced Si particle spheroidization and precipitation of Ni-rich and Al_2Cu phases. The 4 h aged alloy achieved optimal performance, reducing the wear rate by up to 45% with significantly lower friction compared to the as-cast state, whereas over-ageing caused precipitate coarsening and degraded wear behavior.. Studies by dos Santos et al. [14] and Wiengmoon et al. [15] show that heat treatment can facilitate or degrade corrosion resistance markedly based on the continuity, stability, and electrochemical potential of the precipitated intermetallics, which typically serve as active cathodic sites. Moreover, thermal cycling may lead, unintentionally, to surface roughness and modification of a surface energy profile with resultant effect on mechanical properties and local susceptibility of a system to corrosion mechanisms [16]. Therefore, efficient tuning of these coupling parameters is essential for optimising final alloy performance for severe industrial conditions. Notwithstanding extensive research, a notable lack of research is found: a significant lack of multi-response experimental work that examines the combined effects of solution and aging treatment on

[DOI: 10.22068/ijmse.4421]

Al-12Si-Cu alloys with simultaneous microhardness and surface roughness as well as corrosion resistance comparison. In contrast, previous works have mostly focused on mechanical versus electrochemical characteristics individually [17–18]. In an attempt to fill this gap, this study strives to systematically evaluate the impact of four parameters solution temperature 500 °C, 530 °C, solution time 0.5h, 3h, aging temperature 180 °C, 310 °C, aging time 2h, 5h on the microstructure, microhardness, surface roughness, and corrosion behavior of Al-12Si-Cu alloys by adopting the Taguchi L8 orthogonal array design.

2. Experimental setup

2.1 Theory and formula

This work employs Taguchi experimental design. The Taguchi method uses an orthogonal array (OA), a fractional factorial design, to find the best value number of combinations with few experiments taking less time [19]. The Factor and level for process are illustrated in Table 1. It considers solution temperature (500-530°C), solution time (0.5-3 hr), aging temperature (180-310°C), and aging time (2-5 hr). Although, the Taguchi approach requires only 8 experiments to obtain the optimal levels (Table 3) of variables, while to optimize on all factors at two levels, the best solution approach needs 16 tests ($2^4 = 16$), which are practically exhausting. Thus, the Taguchi approach is able to rapid discovery of crucial components, reducing time, money and number of tests [20]. The levels for artificial aging were set at 180 °C and 310 °C. While 180 °C represents the conventional peak-aging temperature for Al-Si-Cu alloys, the higher temperature of 310 °C was strategically selected to investigate the material's behavior under extreme over-aging conditions, which is critical for evaluating the thermal stability of engine components operating at elevated temperatures [21].

[DOI: 10.22068/ijmse.4421]

Table 1: Factor and level for process

Factor	Symbol	Unit	Level	
			Level 1	Level 2
Solution temperature	A	°C	500	530
Solution time	B	hr	0.5	3
Aging temperature	C	°C	180	310
Aging time	D	hr	2	5

As indicated in Table 2, the experiments were carried out with the usual L8 orthogonal matrix based on the Taguchi method by using the statistical program MINITAB 21. The Taguchi method evaluates the quality characteristics using the signal-to-noise (S/N) ratio, where a higher S/N ratio indicates a more robust design. Depending on the type of quality response, three criteria are commonly applied: “larger-is-better,” “nominal-is-better,” and “smaller-is-better.” Each criterion has its own advantages, and the corresponding S/N ratio is calculated according to the following formula [22]:

$$\begin{cases} (S/N)_1 = 10\log(\frac{1}{n}\sum_{i=1}^{n} y_i^2) \\ (S/N)_2 = 10\log(\overline{y}^2/\widehat{\sigma}^2) \\ (S/N)_3 = -10\log(\frac{1}{n}\sum_{i=1}^{n} y_i^2) \end{cases} \qquad \text{……………….(2.1)}$$

In this study, the experimental data were transformed into signal-to-noise (S/N) ratios. The “larger-is-better” criterion was applied for hardness, while the “smaller-is-better” criterion was adopted for surface roughness.

Table 2: L8 design matrix with corresponding experimental results.

[DOI: 10.22068/ijmse.4421]

Exp.	Coded	Un-Coded parameters			
		Solution	Soluti	Aging	Aging
1		500	0.5	180	2
2		500	0.5	310	5
3		500	3.0	180	2
4		500	3.0	310	5
5		530	0.5	180	2
6		530	0.5	310	5
7		530	3.0	180	2
8		530	3.0	310	5

2.2 **Materials**

In this work, an Al–Si–Cu alloy was chosen as the reference (base) material. The chemical composition of the alloy is presented in Table 3. Cylindrical specimens with a diameter of 1.5 cm were cut up and processed. The specimens' surfaces were prepared using a metallographic process (i.e., sequential grinding with silicon carbide (SiC) abrasive papers of different grit sizes, polished with a cloth impregnated with alpha-alumina suspension) to obtain a smooth and reflective surface that can be utilized for microstructure and surface tests before testing.

Table 3 : Chemical composition of Al-Si-Cu alloy.

Element	Si	Cu	Mg	Fe	Zn	Ni	Mn	Ti	Cr	Al
Wt%	12.587	3.563	1.168	0.857	0.683	0.513	0.335	0.070	0.049	Bal.

2.3 **Heat treatment**

The heat-treatment process was designed according to the known principles of solid solution strengthening and precipitation kinetics for Al-Si-Cu alloys. It is done using two steps: solution treatment followed by artificial aging. First, the solution was treated at 500 °C and 530 °C with holding times of 0.5 and 3 hours, respectively, with immediate cold water quenching. This temperature scale was chosen for the purpose of processing at a temperature just below the theoretical eutectic melting point (close to 577°C) for the Al-Si framework, in order to maximise the dissolution of critical hardening phases of the Al matrix (e.g., Al_2Cu and Si), without burning phase locally (local melting) in the alloy structure[23]. The kinetic restriction on phase dissolving was evaluated when the different time varied. Second, the artificial aging was carried out at two temperature ranges (180 °C and 310 °C) of 2 and 5 hours. These temperatures were chosen to represent the two major regimes of precipitation behaviour: 180 °C is the standard peak-age hardening temperature, wherein fine, metastable precipitates are formed maximally to obtain maximum strength. 310°C was adjusted to study precipitation phases under severe over aging, characterized by coarsening of precipitates and non-strengthening phases. It allows a better inspection of the transition from maximum strength to structural stability and deterioration. All the heat treatment procedures developed were performed in a Carbolite 1200-type furnace, which is placed in the Metallurgical Laboratory at the Department of Materials Engineering, University of Technology–Baghdad. The varying heat-treatment schedules were encoded at S0–S8 for clarity and specific conditions were summarized in Table 4.

Table 4 : Conditions of heat treatments.

Specimen Label	Solution Temp.	Solution Time	Aging Temp.	Aging Time
S0	Untreated sample			
S1	500	0.5	180	2
S2	500	0.5	310	5
S3	500	3.0	180	5
S4	500	3.0	310	2
S5	530	0.5	180	5
S6	530	0.5	310	2
S7	530	3.0	180	2
S8	530	3.0	310	5

2.4 **Microhardness and Roughness**

Microhardness testing of untreated and heat-treated samples was conducted with an

[DOI: 10.22068/ijmse.4421]

HVS-1000 microhardness tester (manufactured by LARYEE) using the micro-indentation protocol as recommended by ASTM E384 and ISO 6507 [24]. The indenter was Vickers diamond indent, and the load applied was 9.8 N for 15 sec in constant [25]. Hardness was measured at several locations for each sample, and the average of the values was recorded. Surface roughness measurements were carried out using a TA 620 measuring platform with a handheld roughness gauge (TR200) and a portable roughness gauge (TR240) to accurately capture surface texture. Potentiodynamic polarization tests were performed using a WINKING MLab 200 Potentiostat (Bank-Elektronik, Germany) with a standard three-electrode electrochemical cell. The electrochemical measurements were performed with SCI electrochemical analysis software and carried out at a scan rate of 3 mV/s in which the polarization scans were performed after the open circuit potential Eocp was stabilized. The stabilization criterion was defined in terms of less than 5 mV variation over 10 minutes (as a steady state before polarization) that is congruent with most electrochemical tests. The important electrochemical characteristics obtained were corrosion potential Ecorr and corrosion current density icorr obtained by Tafel extrapolation. The Tafel slopes were also calculated, to further elucidate the anodic and cathodic behavior of the alloy surfaces, across heat treatment conditions.

3. Result discussions

3.1 Microstructures

The as-cast microstructure of Al–Si alloys is composed primarily of large primary α-Al grains, acicular eutectic silicon, and coarse primary silicon particles. Moreover, the formation of adverse intermetallic phases like the needle-like β-Al_5FeSi is found to severely affect the mechanical properties of the alloy [5, 26]. The aluminum in the eutectic phase of unmodified Al–Si alloys displays crystalline features comparable to those of the primary α-Al dendrites

[DOI: 10.22068/ijmse.4421]

[6]. The typical microstructure of the hypoeutectic Al–Si alloy is composed of α-Al grains and dendrites surrounded by eutectic silicon, and is found as elongated acicular structures or as fine rounded particles. The shape of the acicular Si can be changed to a more fibrous shape using suitable chemical modifiers. An optical microstructure of the Al–Si alloy employed in this work is shown in Fig.(1a) and presents the presence of primary α-Al, acicular eutectic Al–Si, and coarse silicon particles [27]. Copper in Al-Si alloys leads to the formation of intermetallic compounds, including Al_2Cu during solidification. This phase may form block-like particles or form lamellar structures that alternate with the α-Al matrix. The Al_2Cu precipitates are often concentrated in the interdendritic area, thereby enhancing mechanical strength. Further, iron could form additional intermetallics like Cu_2FeAl_7 or $Al_5Cu_2Mg_8Si_6$ depending on the specific solidification conditions. The microstructural properties of Al-12Si-Cu alloy were affected by different solution and aging treatments. The untreated sample (S0) had coarse primary α-Al dendrites and long acicular eutectic silicon, as well as intermetallic phases such as blocky Al_2Cu and needle-like β-Al_5FeSi, but significant microstructural refinement occurred after the treatment. Figs (1 a to i) demonstrate the fragmentation, but also partial morphological transformation, of eutectic Si induced by short treatments (e.g., S1 and S2). In comparison, the specimens after prolonged time spent in solution and during aging at a high temperature (e.g., S5–S8) presented more well-homogeneous structures with significant spheroidization of eutectic Si and dissolution of coarse intermetallics. Such two-stage transformation fragmentation followed by spheroidization was especially evident on S8 (530 °C/3h + 310 °C/5h), where the microstructure was completely homogenized with fine, rounded silicon particles dispersed in the α-Al matrix. These findings emphasize that heat-treatment parameters play an essential role in facilitating eutectic Si granulation and refining overall alloy structure and further strengthening mechanical, as well as corrosion-based performance [28]. Additional analysis

[DOI: 10.22068/ijmse.4421]

of heat treatment response for Al-Si-Cu alloy demonstrate that treatment at solution temperature of 500 °C results in a decrease of the average size of silicon particles, which eventually results in fragmented segments turning into a more spheroidal shape. In contrast, treatment at 530 °C for 0.5 hours causes silicon particles to neck, and separate into segments that hold their original shape. Such a partially realized transformation may result in coarsening of eutectic silicon. After treatment with solutions at 530 °C for 3 hours and then aging of the alloy, heterogeneous nucleation is significantly increased– a

[DOI: 10.22068/ijmse.4421]

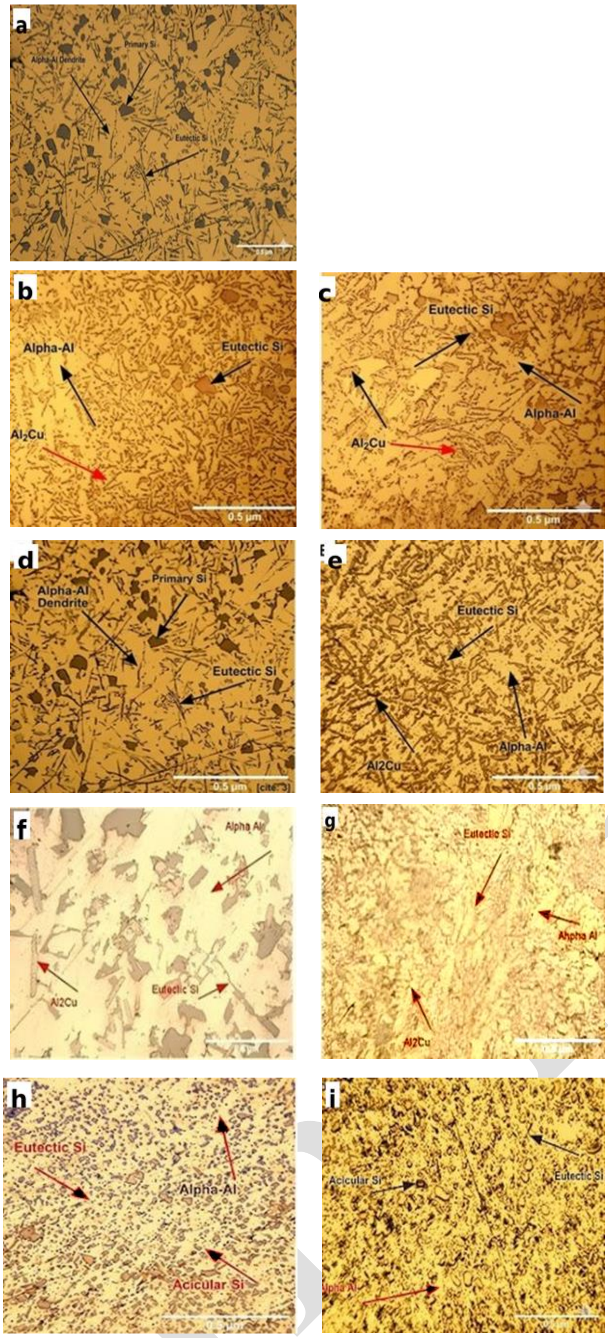

Base metal of Al-Si alloy before heat

Microstructures after heat treatment at 500ºC and 0.5 hrs followed by (b) aging at 180oC for 2hrs, (c) aging at 310ºC for

Microstructures after heat treatment at 500ºC and 3 hrs followed by (d) aging at 180 °C for 5 hrs, and (e) aging at 310 °C

Microstructures after heat treatment at 530ºC and 0.5 hrs followed by: (f) aging at 180 °C for 5 hrs, and (g) aging at 310

Microstructures after heat treatment at 530oC and 3 hrs followed by: (h) aging at 180ºC for 2 hrs. (i) aging at 310ºC for 5

Figure (1): Microstructures after and before heat treatment

dominant factor in grain refinement. The microstructural analysis reveals a significant morphological transformation of the eutectic Si phase. In the as-cast condition, Si particles appear as coarse acicular plates with a high aspect ratio (typically >5). Following the optimized solution treatment at 500 °C, these particles undergo fragmentation and spheroidization, leading to a substantial reduction in the aspect ratio towards a more spherical geometry (approaching 1.5–2.0). Such a process results in nucleation of foreign phases only in specific locations, which grows slowly in molten matrix. Also, when copper, magnesium, and iron are present, there are many intermetallic species produced including Al_2Cu, Mg_2Si, α-$Al_{12}(Fe,Mn)_3Si_2$, and β-Al_5FeSi. Together with the formation of a fine and fibrous eutectic silicon structure through solidification, these compounds significantly affect the mechanical and corrosion performance of the alloy. An Al-Si-Cu alloy precipitation sequence relies on the formation of crystalline Al_2Cu-based precipitates. The Al_2Cu precipitation sequence is described as follows in [9-11]:

$$\alpha_{ss} \rightarrow \text{GP Zones} \rightarrow \theta'' \rightarrow \theta' \rightarrow \theta\ (Al2Cu) \quad ….(3.1)$$

3.2 **Microhardness and Roughness**

Each of the applied heat treatment and aging steps mentioned in Fig.(2) significantly affected the microhardness and surface roughness of the Al-12Si-Cu alloy. The modified Al-Si-Cu alloy microhardness was significantly affected by heat treatment and aging processes. At a fixed solution temperature and holding time, it was observed that lower aging temperatures yielded higher microhardness values. This is probably because the coherent precipitates that form during aging have, by inhibiting dislocation motion, contributed toward the alloy strengthening. By appropriately tuning the aging parameters (temperature and time), an extensive range of mechanical reactions can be obtained [30]. After solution treatment and quenching, the matrix is supersaturated with solute atoms and vacancies. This supersaturation allows fast atomic clustering to result in Guinier Preston (GP) zones. These zones then become metastable coherent or semi-coherent precipitates, either directly or through the dissolution of GP zones, and thus, contribute to strengthening [31].

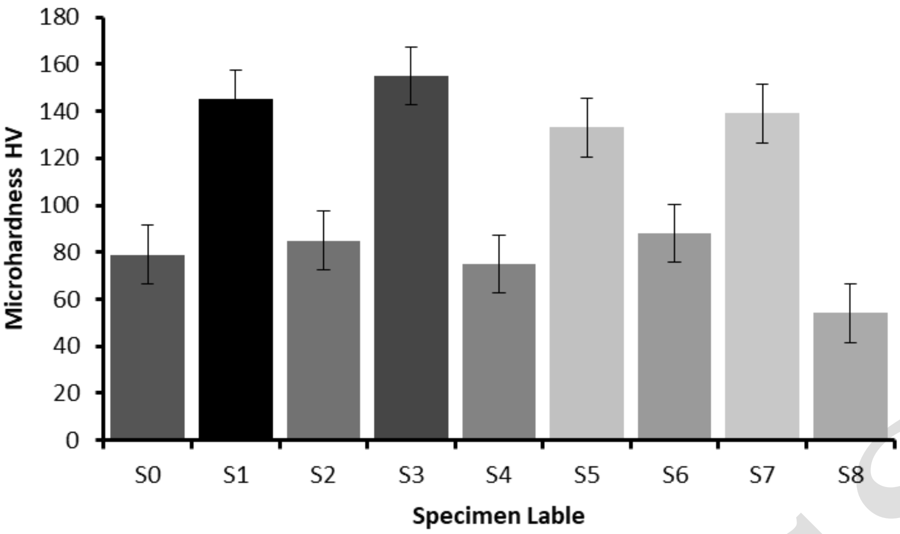

Figure (2): Variation of microhardness with specimen labels

The greatest microhardness value (155 HV) recorded was for specimen S3, which was solution-treated at 500°C for 3 hours and aged at 180°C for 5 hours among testing samples. These results corroborate those of [32]. On the other hand, the low microhardness appeared in specimen S8 (treated at 530°C for 3 hours and aged at 310°C for 5 hours), which may be associated with the over-aging and coarsening of precipitates. S3 was investigated by optical microscopy where good grain refinement, especially in the small sections, is observed which results in high hardness as shown in Fig (3). Moreover, a small increase in surface roughness was observed following heat treatment and aging, which is ascribed to many fine precipitates and small size refinement of the structural phases [33]. The significant decrease in microhardness observed at 310 °C can be attributed to the accelerated precipitation kinetics. According to the precipitation sequence in Al-Si-Cu alloys (αss → GP Zones → θ″→ θ′→ θ) aging at 310 °C promotes the rapid coarsening of the semi-coherent θ′ phase and its subsequent transformation into the coarse, incoherent stable θ (Al2Cu) phase. This transformation leads to a loss of coherency with the aluminum matrix, thereby reducing the pinning effect on dislocation movement [34].

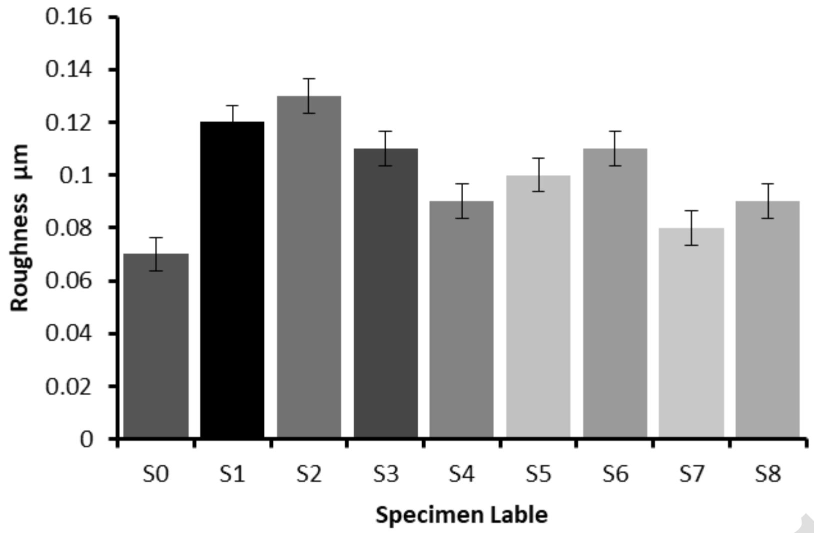

Figure (3): Variation of Roughness with specimen labels

3.3 **Corrosion behavior**

The potentiodynamic polarization curves for unmodified versus heat-treated Al-Si alloys are depicted in Figs (4) and (5). These curves have two specific actions in the active region. The lower curve is the cathodic reaction, namely the reduction of the dissolved oxygen, denoted by this reaction:

$$O2 + 2H2O + 2e \rightarrow 4OH^{-} \text{ …… (4.1).}$$

On the contrary, the upper part of the polarization curve denotes the anodic reaction, and is where the oxidation of aluminum alloy takes place. Typically, this reaction is described as follows:

$$Al \rightarrow Al3+ + 3e \text{ …….. (4.2).}$$

Changes in the anodic and cathodic branches of treated and untreated samples may demonstrate the effects of heat treatment on corrosion behaviour, passive film stability, and

[DOI: 10.22068/ijmse.4421]

electrochemical properties of the precipitated intermetallic phases. Table (5) The potentiodynamic polarization results, which are summarized, show that the corrosion behavior in these specimens varies significantly from one another. The untreated sample, S0, presented a corrosion potential (Ecorr) of (– 611 mV) and a corrosion rate (CR) of 32.48 mpy, providing a reference sample to compare performance. The thermal regime was applied for each of the studied classes and significant variations followed the heat treatment. Among the specimens treated at 500°C, S1 (0.5h + aging at 180°C for 2h) showed a significant change in the corrosion performance, Ecorr = – 679 mV and CR = 4.76 mpy, signifying good corrosion resistance and improved microhardness (145 HV) compared to S0. Conversely, S3 (500°C at 3h plus aging at 180°C at 5h) had the greatest hardness (155 HV) and moderate roughness (0.11 μm), and the high corrosion (35.07 mpy) rate, indicating effective mechanical strength-corrosion compromise. Specimen S4 experienced worst performance against corrosion, despite treatment at 500°C for a period of 3h and aging at 310°C for two h, because of corrosion capacity at CR= 142.89 mpy, probably reflecting coarsened intermetallics as galvanic couples. At 530°C, S5 (0.5h + aging with 180°C for 5h) and S7 (3h + aging with 180°C for 2h) had a better balance between the two values, in particular for S7 the most noble Ecorr = – 436 mV with CR = 17.32 mpy indicating better passivation but moderate corrosion rate. S8 had the weakest hardness (54 HV), and achieved negligible corrosion resistance (CR = 31.63 mpy), suggesting it was suboptimal. Taking into account the three main parameters, hardness, roughness, and rate of corrosion, S1 has the best combination and provides good corrosion resistance, adequate hardness, and moderate surface roughness. Overall, there was a modest influence of heat treatment on the corrosion behavior and considerable differences can be explained by the appearance or dissolving of specific microstructural features. For 500°C, short solution treatment (0.5h) with aging facilitated a decrease in corrosion rates, possibly caused by the formation of Guinier–Preston

(GP) zones and coherent/semi-coherent precipitates to reduce microgalvanic coupling. But the long-term treatment (3h), the zones might become dissolved and the susceptibility to the corrosion would grow. On the contrary, at 530°C the solution time increased to a total of 3h which led to lower corrosion rate due to improved intermetallic refinement and eutectic Si fragmentation with respect to optical and roughness data. This delicate microstructure also resulted in lower localised anodic/cathodic sites and attenuated corrosion evolution [12,13,35].

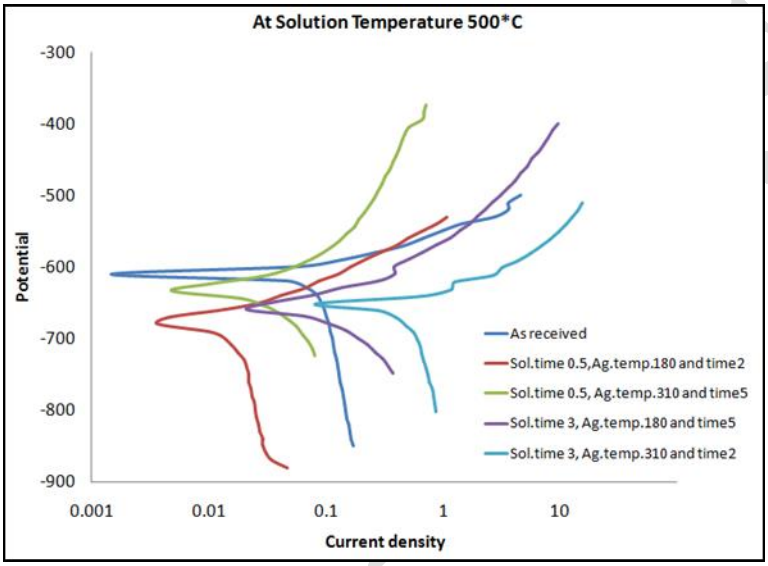

Figure (4): Tafel polarization plots of as-received and heat-treated specimens at 500 °C solution temperature with varying solution times (h), aging temperatures (°C), and aging times (h).

Moreover, high surface roughness reported among specimens (e.g., S2) may also relate to enhanced susceptibility to corrosion as rough surfaces offer more active sites for electrolyte penetration and localized corrosion. As a result, the hardness, roughness, and microstructural refinement are balanced to improve corrosion resistance. Specimen S2 displayed the greatest surface roughness (0.13 µm), which may relate to coarse intermetallic phases formation from aging at 310 °C for 5 h. S8 demonstrated only moderate roughness (0.09 µm) despite having the lowest hardness (54 HV), which supports the possibility that the

[DOI: 10.22068/ijmse.4421]

thermal conditions may have resulted in spheroidization and consequently did not prevent precipitation hardening. The potentiodynamic polarization results (Table 5) indicate that corrosion had different performances among observed samples. For example, the sample S0 presented a corrosion potential Ecorr and corrosion rate (CR) of −611 mV and 32.48 mpy, respectively, used as an intermediate sample to compare the corrosion behavior. When heat was applied, prominent changes were found according to the application temperature. For 500 °C-treated samples, S1 (0.5h) + aging at 180°C for (2 h) resulted in remarkable improvement, as evidenced by Ecorr= –679 mV and CR = 4.76 mpy, with good corrosion resistance and superior microhardness (145 HV) to S0. Notably, an absolute compromise between mechanical performance and corrosion protection was obtained. Accordingly, S3 (500°C for 3 h + aging at 180 °C for (5 h)) showed the highest hardness (155 HV) but a much higher corrosion rate (35.07 mpy). This indicates that the particular thermal conditions that favor the optimal precipitation strength may also facilitate the formation of closer and more continuous networks of micro-galvanic sites. In contrast, the worst corrosion performance (CR = 142.89 mpy) occurred in S4, which was treated for (3 h) at 500°C but aged for (2 h) at 310°C, probably due to coarsened intermetallics being very efficient galvanic couples. S7 (3h + aging at 180°C) at 530°C for (2h) had the most noble Ecorr = – 436 mV and a moderate corrosion rate (17.32 mpy) indicating better passivation. Following the trend, in addition, S8 exhibited the lowest hardness (54 HV) and no visible corrosion property improvements (CR = 31.63 mpy), verifying its sub-optimal performance. Mechanics: Microstructure and corrosion. Corrosion resistance is determined by the morphological variation resulting from the heat treatment. The effect of heat treatment on the corrosion behavior is moderate in nature but complicated. At 500°C, shorter solution treatment (0.5h) and aging (S1) contribute to reduced corrosion rates, which might be attributed to the formation of fine Guinier–Preston (GP) regions and coherent precipitates. By consuming local Cu atoms contained in the matrix,

[DOI: 10.22068/ijmse.4421]

these fine precipitates form a solute-depleted region adjacent to the particles. Such a region effectively diminishes the differential driving micro-galvanic coupling present in the system. But long-term treatment (3h) may cause these areas to dissolve or coarsen, increasing vulnerability. By contrast, conditions that induced reduced corrosion rates, especially those with a higher 530 °C solution temperature and longer times (e.g., S7), showed improved intermetallic refinement and eutectic Si fragmentation. This change is visually supported by the optical and roughness data, which describes a more streamlined microstructure that has a huge role in the cause of the corrosion. Si spheroidization (the process requested by the reviewer) plays an important role here, in that it breaks the continuous linear path of the Si eutectic network to form a lot more small (isolated) particles of the large, continuous cathodic network. Such morphological change efficiently lowers active surface area for the cathodic phase and shrinks the length scale over which galvanic cells can function, resulting in lesser localized anodic/cathodic sites and reducing corrosion propagation. Moreover, some specimens (e.g., S2, 0.13 μm) exhibit greater surface roughness, which can also be an indicator for increased susceptibility to corrosion; a rougher surface allows for more active sites for electrolyte penetration and localized corrosion. So, the ultimate corrosion resistance is reached through the interplay of precipitation hardening, which may enhance galvanic coupling, with microstructural refinement and Si spheroidization, the action of which physically impedes the cathodic routes.

Table 5: Properties of Al-Si alloy before and after heat treatments.

Specimen Label	Microhardness HV	Roughness μm	Ecorr mV	icorr μA/cm2	CR mpy
S0	79	0.07	-611	75	32.48
S1	145	0.12	-679	11	4.76

[DOI: 10.22068/ijmse.4421]

S2	85	0.13	-634	24	10.39
S3	155	0.11	-657	81	35.07
S4	75	0.09	-651	330	142.89
S5	133	0.10	-706	190	82.27
S6	88	0.11	-574	312	135.10
S7	139	0.08	-436	40	17.32
S8	54	0.09	-681	73	31.63

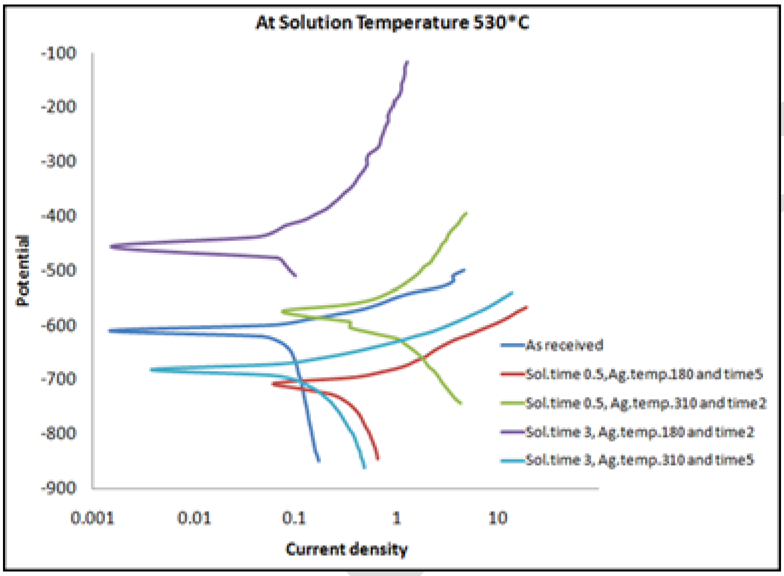

Figure (5) :Tafel polarization plots of as-received and heat-treated specimens at 530 °C solution temperature with varying solution times (h), aging temperatures (°C), and aging times (h).

3.4 **Optimization and statistical analysis (Taguchi method)**

3.4.1 **Probability Plots**

A probability plot is a very easy way to find out if a data set satisfies a hypothesized distribution. The data are plotted against an ideal distribution and if the plot is a straight line, it can reasonably be assumed that the observed statistical sample is from the ideal distribution. Variations away from that line are departures from the distribution. To test for normality assumption of the experimental data, the Anderson-Darling test (ADT) is applied. The ADT is an efficient statistical tool to detect deviations from normality and is particularly useful to study outliers [36]. Fig.6 tells us, as shown, that these data are nearly in the straight line and the p-value is greater than 0.05. That means we have a normal distribution for the experimental data indicating its potential for further study and refinement.

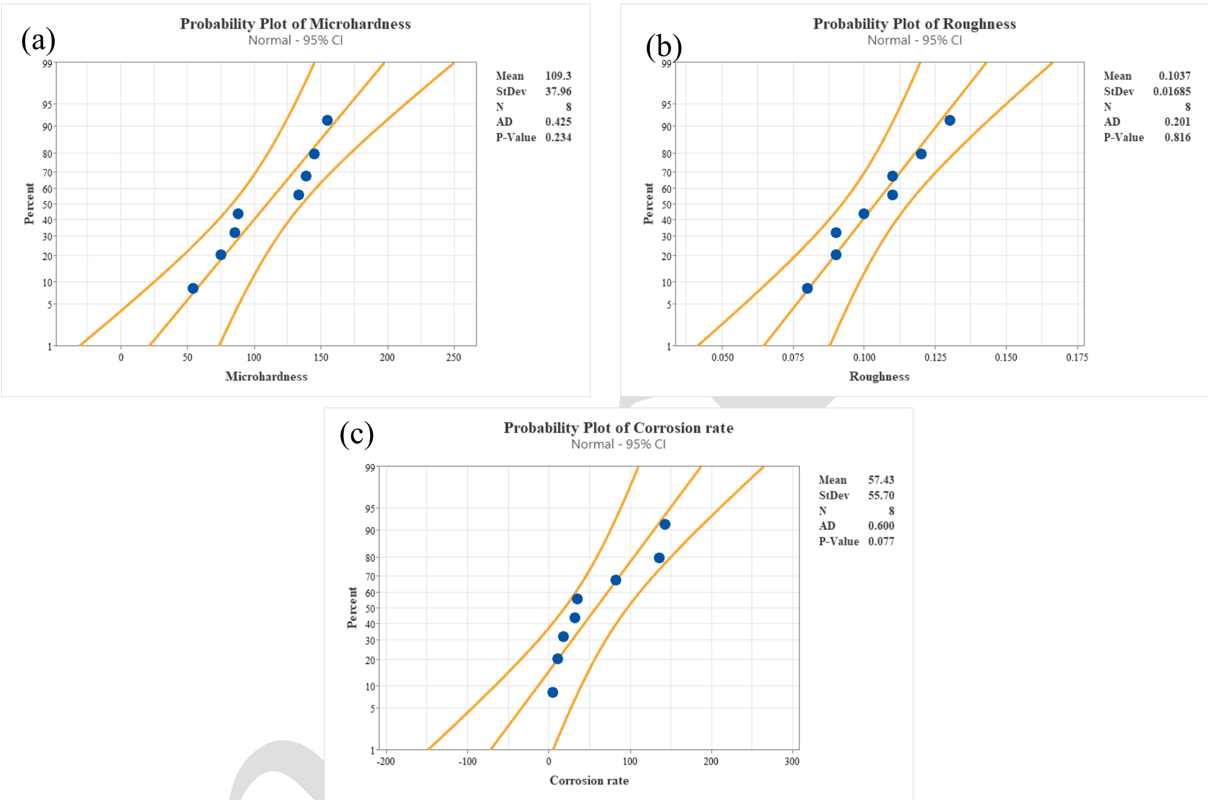

Figure (6):Probability Plot of (a) Microhardness, (b) Roughness, (c) Corrosion rate.

3.4.2 Mean Effects plot for means

The main effect plots of the composite are depicted in Fig.(7), and the main effect plot for mean hardness as shown in fig.(7-a) indicates that hardness decreases with increase in solution temperature, solution time, aging temperature, and aging time (500-530°C, 0.5-3 hr,180-310°C, 2-5hr). For mean roughness, fig.(7-b) shows the main effect plot which indicates that roughness increases with increase in solution temperature, aging temperature, and aging time (500-530°C,180-310°C, 2-5hr) and decreases linearly with increase in solution time (0.5-3). Finally, see the main effect plot for mean corrosion rate from fig.(7-c) depicting how corrosion rate increases with increase in solution temperature and aging temperature (500-530°C,180-310°C). Also, corrosion rate decreases linearly with increase of solution time and aging time (0.5-3, 2-5) hr.

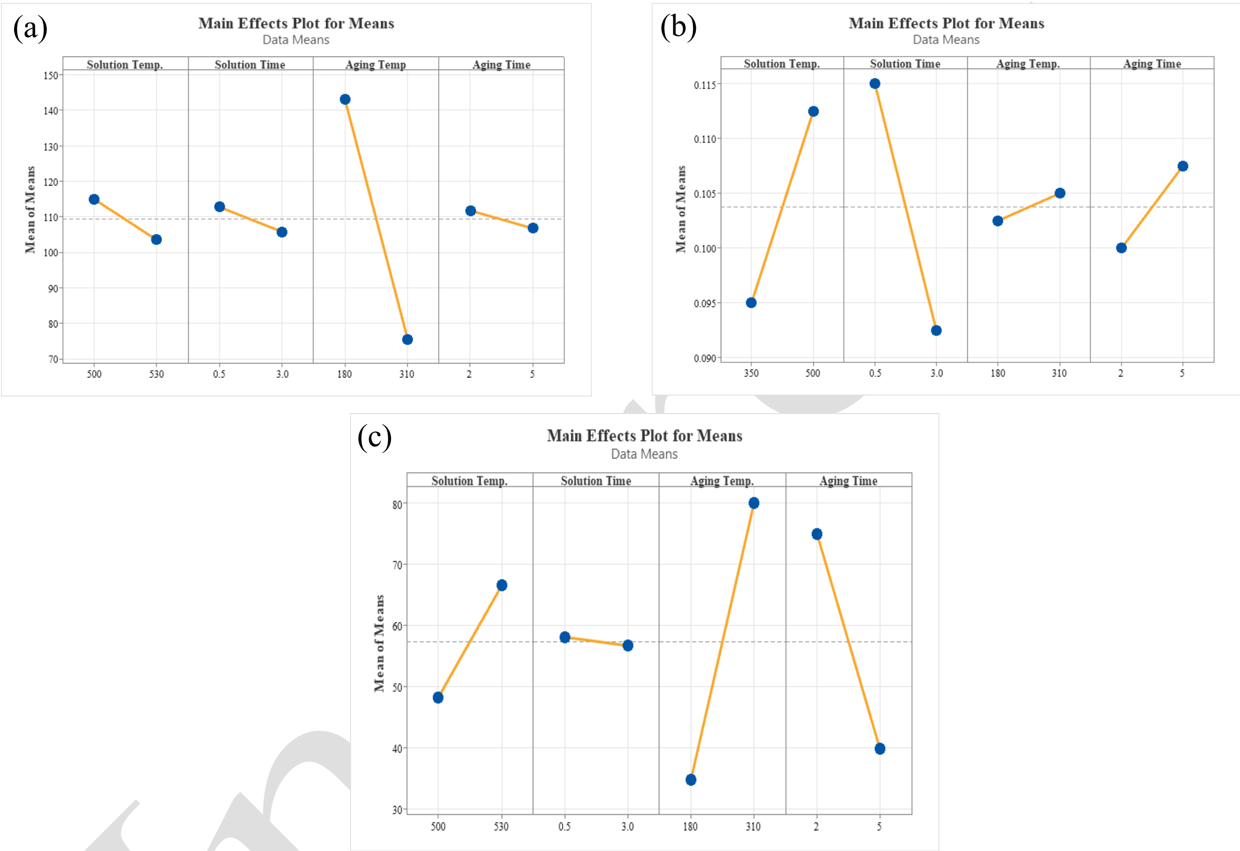

Figure(7):Mean effect plot for mean of (a) Microhardness, (b) Roughness, (c) Corrosion rate.

3.4.3 Single Objective Optimization

Individual responses are optimized in terms of signal to noise (S/N) ratios[37]. In this study, we have several functions for individual responses, namely maximizing hardness and minimizing both corrosion rate and roughness. Therefore, Equation (1) is used to apply the "larger is better" property for hardness, and Equation (2) is used for corrosion rate and roughness. The signal-to-noise ratio for each factor is shown in Table 6 using the MiniTab21

[DOI: 10.22068/ijmse.4421]

analytical program. Regarding the signal-to-noise ratio (SNR) for the hardness test, as mentioned in Table 6, the highest SNR was 43.8066 for Experiment 3, which had (solution temperature, aging temperature, and aging time at Level 1, respectively, and solution time at Level 2). For roughness, the highest SNR was noted for Experiment 7 (21.9382), which had (solution temperature, solution time, and aging time at Level 2, and aging temperature at Level 1). Finally, for corrosion rate, the highest SNR was -13.5521 for Experiment 1, which had (solution temperature, solution time, aging temperature, and aging time at Level 1, respectively). The optimum levels were obtained from the average signal-to-noise ratios, as shown in Fig.(8). For hardness, all factors were optimal at Level 1. For roughness, three factors (solution temperature, aging temperature, and aging time) were optimal at Level 1, while solution time was optimal at Level 2. For corrosion rate, three factors (solution temperature, solution time, and aging temperature) were optimal at Level 1, whereas aging time was optimal at Level 2.

Table 6: Results Signal to noise ratio using for each test L8 OA

Experimental	Signal to noise ratio		
	Hardness test	Roughness	Corrosion rate
1	43.2274	18.4164	-13.5521
2	38.5884	17.7211	-20.3323
3	43.8066	19.1721	-30.8987
4	37.5012	20.9151	-43.1000
5	42.4770	20.0000	-38.3048
6	38.8897	19.1721	-42.6131
7	42.8603	21.9382	-24.7710
8	34.6479	20.9151	-30.0020

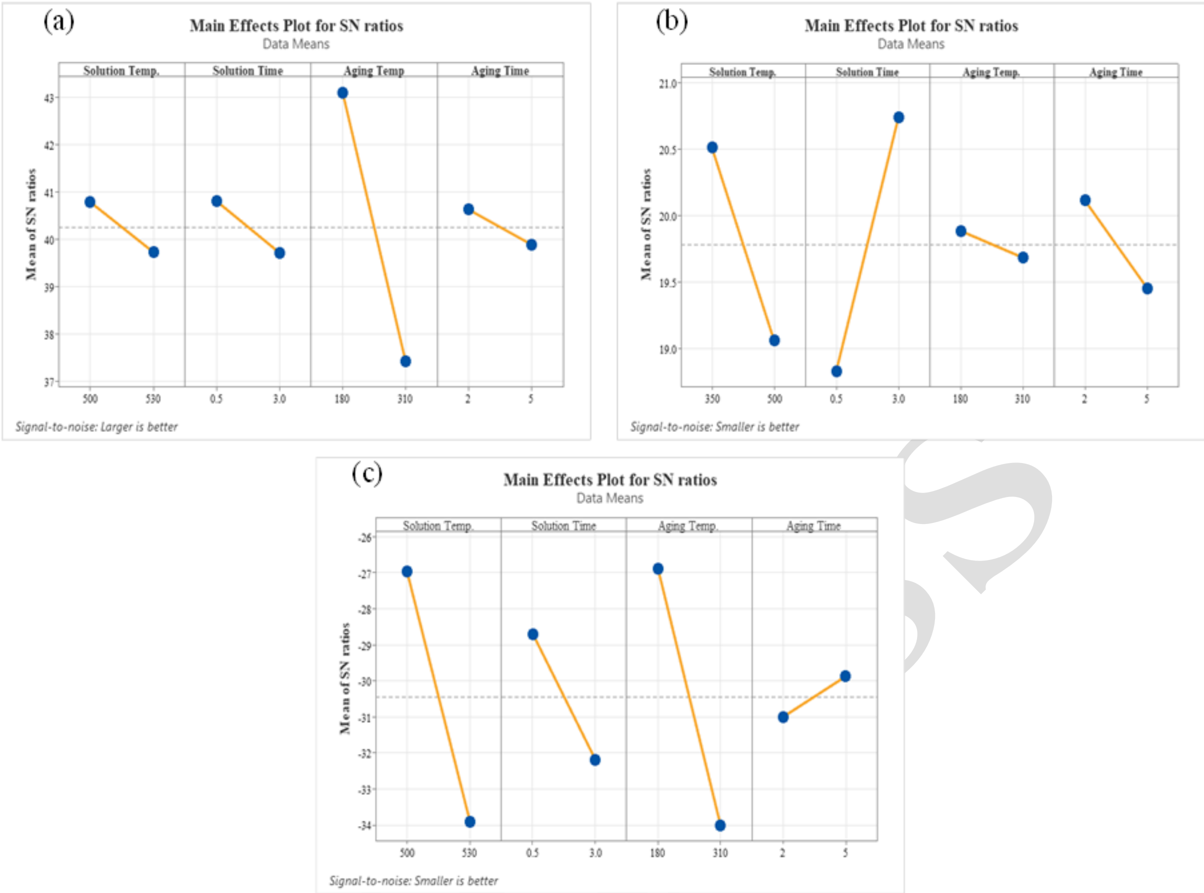

Figure (8) : Main effects plots for the signal-to-noise (S/N) ratios of (a) Microhardness, (b) Surface roughness, and (c) Corrosion rate.

3.4.4 Analysis of Variance

The main purpose of the Analysis of Variance (ANOVA) was to obtain an estimate of the magnitude and impact of each heat treatment parameter on the final material properties. Analysis was performed within a 95% confidence interval. Normally, a $P < 0.05$ is needed to show statistical significance of a factor. The ANOVA results (Table 7) presented showed that P-values for most of the 3 factors (microhardness of the material, surface roughness of the material and corrosion rate) were greater than 0.05. This result — common to Taguchi L8 orthogonal array designs, which make minimal use of degrees of freedom for error estimation — implies that, although the factors are not universally statistically significant at the 95% confidence level in this particular experimental model, the analysis will be key for

[DOI: 10.22068/ijmse.4421]

unveiling the prevailing trends and the relative hierarchy of factor influence [38]. The percentage contribution does not show statistical significance, but provides significant information about the underlying physics of the process:

- Microhardness: The aging temperature (84.152%) was the most contributing factor, which goes hand-in-hand with precipitation kinetics as the strongest mechanism for strength enhancement. Next, were solution time (3.101%), solution temperature (2.936%) and aging time (1.423%).
- Surface roughness: The solution time (51.548%) dominated the outcome, and solution temperature (29.786%) was two main contributors, indicating that final surface quality is largely dependent upon the dissolution and microstructural homogenization.
- Corrosion rate: Aging temperature (12.8671%) and solution temperature (12.231%) played an almost equal role and demonstrated complex interaction of precipitation morphology and phase dissolution on electrochemical behavior.

The error contribution in the ANOVA analysis (approximately [X]%) is attributed to uncontrollable factors such as minor fluctuations in furnace temperature and the inherent variability in the manual polishing process during microstructure preparation. Since the Taguchi L8 design focuses on main effects, the interaction terms were pooled into the error term, confirming that the individual parameters, especially aging temperature, are the primary drivers of the alloy’s performance. The best condition of the results suggest a compromise between the mechanical and corrosion properties. For S1, the lowest corrosion rate (4.76 mpy) was attained and the highest hardness (155 HV) at S3. Upon analysing multi-objective optimization (Taguchi S/N and ANOVA analyses for all responses), the analysis is able to deduce the different processing windows to maximize each property, guiding future engineering activities. Therefore, the ideal responses are adapted to suit the end-use - the S3

[DOI: 10.22068/ijmse.4421]

design is optimal for strength applications and S1 for corrosion requirements. The enhancement in corrosion resistance (4.76 mpy) is attributed to two synergistic effects. First, the spheroidization of eutectic Si particles reduces the number of sharp edges, which typically act as localized cathodic sites for pit initiation. Second, the optimized heat treatment leads to a more uniform distribution of Cu-rich intermetallics, minimizing the formation of severe galvanic couples between the α-Al matrix and the precipitates. According to the ANOVA results, aging temperature was the most influential factor, as it controls the degree of Cu-precipitation and the subsequent electrochemical stability of the alloy surface.

Table 7 : ANOVA results

Test	Source	DF	Seq SS	Adj SS	Adj MS	F	P	%Concentration
Hardness test	Solution	1	2.256	2.256	2.256	1.05	0.381	2.936
	Solution	1	2.383	2.383	2.383	1.11	0.369	3.101
	Aging	1	64.662	64.662	64.662	30.11	0.012	84.152
	Aging	1	1.094	1.094	1.094	0.51	0.527	1.423
	Residual	3	6.443	6.443	2.148			8.385
	Total	7	76.839					
Roughness test	Solution	1	4.2060	4.20600	4.20600	7.47	0.072	29.786
	Solution	1	7.2790	7.27900	7.27900	12.94	0.037	51.548
	Aging	1	0.0806	0.08063	0.08063	0.14	0.730	0.57
	Aging	1	0.8669	0.86688	0.86688	1.54	0.303	6.139
	Residual	3	1.6882	1.68821	0.56274			11.955
	Total	7	14.1207					
Corrosion rate	Solution	1	96.658	96.658	96.658	0.51	0.525	12.231
	Solution	1	24.393	24.393	24.393	0.13	0.743	3.0868
	Aging	1	101.679	101.679	101.679	0.54	0.516	12.8671
	Aging	1	2.529	2.529	2.529	0.01	0.915	0.3200
	Residual	3	564.962	564.962	188.321			71.494
	Total	7	790.222					

4. Conclusions

According to a combined study of the heat treatment, microstructure, hardness, surface roughness, corrosion characteristics of Al-12Si-Cu alloy, the following conclusions are deduced:

1. Microstructural control: Heat treatment and aging are the most applicable to engineered microstructure. The procedure also successfully promoted intense segmentation and spheroidization of the eutectic silicon (Si) phase and the conversion of coarse primary intermetallic particles into a more refined and uniformly distributed morphology.

2. Mechanical Properties: The alloy mechanical properties are highly dependent on controllable precipitation kinetics. The highest microhardness (155 HV) occurred in the S3 condition (500 °C 3 h + 180 °C 5 h), optimal for maximum precipitation hardening. The lowest hardness (54 HV) also indicates that prolonged ageing at high aging temperature (530 °C 3h + 310 °C 5h) results in severe over age and related loss of strength.

3. The corrosion behavior is microstructural state dependent and characterized by its mechanisms and performance. For specimen S1 (500°C 0.5h + 180°C 2h), the most satisfactory corrosion resistance (lowest corrosion rate of 4.76 mpy) was recorded. This improvement can mainly be traced to the enhancement of the microstructure and spheroidization of the eutectic Si network, which effectively alters the continuous cathodic path and reduces micro-galvanic coupling, thus inhibiting corrosion growth.

4. Trade-Off and Factor Effects: The results show a clear trade-off between the conditions that enhance hardness (e.g., S3) and those which reduce corrosion resistance; and vice versa. Based on Taguchi analysis, the aging temperature was identified as the most important parameter that controlled the mechanical, as well as corrosion properties, with

[DOI: 10.22068/ijmse.4421]

solution time considered more in proportion to factor performance, indicating the importance of thermal kinetics.

5. Optimization Results: The particular processing windows for each optimal target property are adequately defined in this work. The ultimate conditions for the maximum strength (S3) and the best corrosion protection (S1) are well characterized and will offer useful recommendations for the industrial applications of Al-12Si-Cu alloys.

Acknowledgements

The authors would like to express their gratitude to the Southern Technical University and the Middle Technical University for providing the laboratory facilities and technical support necessary to conduct the experimental part of this research.

References

[1] Dash, S. S. and Chen, D., "A Review on Processing–Microstructure–Property Relationships of Al–Si Alloys: Recent Advances in Deformation Behavior." Metals, 2023, 13, 609.

[2] Eshaghi, A., Ghasemi, H. M. and Rassizadehghani, J., "Effect of Heat Treatment on Microstructure and Wear Behavior of Al–Si Alloys with Various Iron Contents." Mater. Des., 2011, 32, 1520–1525.

[3] Nnakwo, K. C., Nwajioke, C. T., Chukwuneke, J. L., Ugwuanyi, B. C., Ogbunaoffor, K. C. and Ozoh, C. C., "Microstructure Evolution in A356 Alloy Subjected to Controlled Heat Treatment Regimes Processes." Discov. Appl. Sci., 2024, 6, 497.

[4]] Callegari, B., Lima, T. N. and Coelho, R. S., "The Influence of Alloying Elements on the Microstructure and Properties of Al–Si-Based Casting Alloys: A Review." Metals, 2023, 13, 1174.

[5] Mohamed, A. M. A. and Samuel, F. H., “Heat Treatment of Al–Si–Cu/Mg Casting Alloys.” In: Heat Treatment: Conventional and Novel Applications, 2012, 55.

[6] Zhang, N “Microstructure Evolution and Mechanical Properties of Al–12Si–xCu–yNi–1Mg Alloy with Different Ni/Cu Ratios.” Mater. Today Commun., 2024, 38, 108081.

[7] Abdelaziz, M. H., Elgallad, E. M., Doty, H. W. and Samuel, F. H., “Strengthening Precipitates and Mechanical Performance of Al–Si–Cu–Mg Cast Alloys Containing Transition Elements.” Mater. Sci. Eng. A, 2021, 820, 141497.

[8] Zhang, M., Tian, Y., Zheng, X., Zhang, Y., Chen, L. and Wang, J., “Research Progress on Multi-Component Alloying and Heat Treatment of High Strength and Toughness Al–Si–Cu–Mg Cast Aluminum Alloys.” Materials, 2022, 12, 1065.

[9] Xie, Y., Liu, S., Guo, X. and Deng, Y., “Development of Ultra-High Strength Al–Cu–Li Alloys Containing High Mg through the Combination of Pre-Stretching and Age-Hardening.” Mater. Sci. Eng. A, 2024, 896, 146289.

[10] Sinnwell, Y., Maksakov, A., Palis, S. and Antonyuk, S., “Influence of the Particle Morphology on the Spray Characteristics in Low-Pressure Cold Gas Process.” Powder Technol., 2025, 464, 121084.

[11] Bahl, S., Xiong, L., Allard, L. F., Michi, R. A., Poplawsky, J. D., Chuang, A. C., Singh, D., Watkins, T. R., Shin, D., Haynes, J. A. and Shyam, A., “Aging Behavior and Strengthening Mechanisms of Coarsening Resistant Metastable θ' Precipitates in an Al–Cu Alloy.” Mater. Des., 2021, 198, 109378.

[12] Pezda, J., “The Effect of the T6 Heat Treatment on Hardness and Microstructure of the EN AC-AlSi12CuNiMg Alloy.” Metalurgija, 2014, 53, 63–66.

[13] Raju, K., Jagadeesha, T., Alavandi, M. R., Kurahatti, R. V. and Goudar, D. M., “Effect of Aging Time on the Microstructure and the Wear Behavior of Al–15Si–6Ni–2Cu Alloy.” J. Mater. Eng. Perform., 2026.

[DOI: 10.22068/ijmse.4421]

[14] dos Santos, S. L., Tolockzo, F. R., Merij Neto, A. C., Cezario, F. E. M., da Silva, D. M. and Antunes, R. A., “Microstructural Evolution and Corrosion Behavior of Non-Isothermally Heat Treated Hypoeutectic Al–Si–Cu Alloy.” Next Mater., 2024, 5, 100262.

[15] Wiengmoon, A., Sukchot, P., Tareelap, N., Pearce, J. T. H. and Chairuangsri, T., “Effects of T6 Heat Treatment with Double Solution Treatment on Microstructure, Hardness and Corrosion Resistance of Cast Al–Si–Cu Alloy.” Arch. Metall. Mater., 2015, 60, 881–886.

[16] Xie, D., Wang, Z., Zhou, X., Cheng, X. and Li, X., “Effect of Different Laser Energy Densities on the Corrosion Resistance of Aluminum Alloys.” Anti-Corros. Methods Mater., 2020, 67, 437–444.

[17] Korkmaz, A., Yağcı, T. and Çulha, O., “A Computational and Experimental Approach to the Enhancement of Heat Treatment Processes for Al–Si–Mg Alloys.” J. Alloys Compd., 2025, 1035, 181468.

[18] Cabrini, M., Lorenzi, S., Testa, C., Pastore, T., Manfredi, D., Lorusso, M., Calignano, F. and Fino, P., “Statistical Approach for Electrochemical Evaluation of the Effect of Heat Treatments on the Corrosion Resistance of AlSi10Mg Alloy by Laser Powder Bed Fusion.” Electrochim. Acta, 2019, 305, 459–466.

[19] [19] Bayati, A., Ahmadi, M., Rahmatabadi, D., Khodaei, M., Xiang, H., Baniassadi, M., Abrinia, K., Zolfagharian, A., Bodaghi, M. and Baghani, M., “3D Printed Elastomers with Superior Stretchability and Mechanical Integrity by Parametric Optimization of Extrusion Process Using Taguchi Method.” Mater. Res. Express, 2025, 12, 015301.

[20] Shojaei, S., Shojaei, S., Band, S. S., Kazemzadeh Farizhandi, A. A., Ghoroqi, M. and Mosavi, A., “Application of Taguchi Method and Response Surface Methodology

[DOI: 10.22068/ijmse.4421]

into the Removal of Malachite Green and Auramine-O by NaX Nanozeolites.” Sci. Rep., 2021, 11, 16054.

[21] Jung, J.-G., Park, J.-S. and Lee, Y.-K., “Quantitative Analyses of Dissolution and Precipitation Kinetics of θ-Al_2Cu Phase in an Al-6.2Si-2.9Cu Alloy Using Electrical Resistivity.” Metals Mater. Int., 2013, 19, 147–152.

[22] Wu, H., Li, H., Wang, X., Yang, J., Jiang, R., Deng, X. and Wang, J., “Research on Multi-Objective Optimization Design for High-Precision Turning-Milling Machine Tool Bed Based on Taguchi Method–FEA.” Sci. Rep., 2025, 15, 27307.

[23] Jang, J.-H., Nam, D.-G., Park, Y.-H. and Park, I.-M., “Effect of Solution Treatment and Artificial Aging on Microstructure and Mechanical Properties of Al–Cu Alloy.” Trans. Nonferrous Met. Soc. China, 2013, 23, 631–635.

[24] International Organization for Standardization, “Metallic Materials—Vickers Hardness Test—Part 1: Test Method (ISO 6507-1:2018).” ISO, Geneva, 2018.

[25] Eqal, A. K., Yagoob, J. A. and Hussein, H. A., “Investigation of the Effect of TiC on Some Properties of ZA-27 Alloy Prepared by Powder Metallurgy Method.” Mater. Res., 2024, 27, e20240143.

[26] Zhao, G., Xing, Z., Li, M., Gao, S., Tao, J. and Chai, S., “Research on Microstructure and Growth Mechanism of Different Primary Silicon in Hypereutectic Aluminum Alloy.” J. Phys. Conf. Ser., 2022, 2152, 012022.

[27] Rashed, H. M. M. A., Ashrafi, E. A. and Hasan, A., “Modelling Effects of Copper on Microstructure and Properties of Al–Si–Cu Alloys.” Mater. Trans., 2023, 64, 177–183.

[28] Sivarupan, T., Taylor, J. A. and Cáceres, C. H., “Effect of Si and Cu Content on the Size of Intermetallic Phase Particles in Al-Si-Cu-Mg-Fe Alloys.” In: Shape Casting: 5th International Symposium, 2014, 161–168.

[DOI: 10.22068/ijmse.4421]

[29] Ibrahim, A. I., Elgallad, E. M., Samuel, A. M., Doty, H. W. and Samuel, F. H., "Effects of Addition of Transition Metals on Intermetallic Precipitation in Al–2%Cu–1%Si-Based Alloys." Int. J. Metalcast., 2018, 12, 574–588..

[30] Ringer, S. P. and Hono, K., "Microstructural Evolution and Age Hardening in Aluminium Alloys: Atom Probe Field-Ion Microscopy and Transmission Electron Microscopy Studies." Mater. Charact., 2000, 44, 101–131.

[31] Wang, H., Deng, W. and Wang, S., "Precipitates Generation Mechanism and Surface Quality Improvement for Aluminum Alloy 6061 in Diamond Cutting." J. Wuhan Univ. Technol. Mater. Sci. Ed., 2024, 39, 150–159.

[32] Sui, Y., Jiang, Y. and Wang, Q., "Effect of Solution Treatment on Microstructure and Mechanical Properties of As-Cast Al-12Si-4Cu-2Ni-0.8Mg-0.2Gd Alloy." China Foundry, 2022, 19, 238–244.

[33] Amith, V. K., Baloor, S. S., Polishetty, A., Bolar, G. and Govindhan, A. N., "Heat Treatment and Its Effect on Machining Induced Surface Roughness of Cast and Additive Manufactured AlSi10Mg." Sci. Rep., 2025, 15, 26433.

[34] Heugue, P., Larouche, D., Breton, F., Massinon, D., Martinez, R. and Chen, X.-G., "Precipitation Kinetics and Evaluation of the Interfacial Mobility of Precipitates in an AlSi7Cu3.5Mg0.15 Cast Alloy with Zr and V Additions." Metals, 2019, 9, 777.

[35] Rocha, W. F. C., Prado, C. B. and Blonder, N., "Comparison of Chemometric Problems in Food Analysis Using Non-Linear Methods." Molecules, 2020, 25, 3025.

[36] Qazi, M. I., Akhtar, R., Abas, M., Khalid, Q. S., Babar, A. R. and Pruncu, C. I., "An Integrated Approach of GRA Coupled with Principal Component Analysis for Multi-Optimization of Shielded Metal Arc Welding (SMAW) Process." Materials, 2020, 13, 3457.

[37] Lingam, D., Ananthanarayanan, R., Jeevanantham, A. K. and Seenivasagam, D. R., "Optimization Methods in Powder Metallurgy for Enhancing the Mechanical Properties: A Systematic Literature Review." Eng. Res. Express, 2024, 6, 022504.